Exceptional Near Infrared Fluorescence Quantum Yields and Excited-State Absorptivity of Highly Conjugated Porphyrin Arrays

Timothy V. Duncan, Kimihiro Susumu, Louise E. Sinks, and
Michael J. Therien*
Department of Chemistry, University of Pennsylvania
Philadelphia, Pennsylvania 19104-6323

Supporting Information Section

Synthesis. The synthesis and characterization of **DD, DA, DDD, DAD, DDDDD** and **DADAD** have been reported previously.[1]

Instrumentation. Electronic spectra were recorded and ground-state molar extinction coefficients were determined using both a Shimadzu PharmaSpec UV1700 spectrophotometer and an OLIS UV/vis/near-IR spectrophotometry system that is based on the optics of a Cary 14 spectrophotometer. Emission spectra were recorded on a SPEX Fluorolog 3 luminescence spectrophotometer that utilized a T-channel configuration with red sensitive R2658 Hamamatsu PMT (300 nm – 850 nm) and liquid nitrogen cooled InGaAs detectors (850 nm – 1500 nm); these spectra were corrected using the spectral output of a calibrated light source supplied by the National Bureau of Standards.

Ultrafast Transient Absorption Experiments. Transient absorption spectra were acquired using standard pump-probe methods. A schematic of this transient optical system and detailed description of the apparatus is provided in the Supporting Information section of reference 2. Probe light at wavelengths up to 1.4 μm were generated by the method described previously[2]; to access the 1.4-1.8 μm region of the near-IR (NIR), probe pulses were generated in a 3 mm thick sapphire disk with 1.9 μm light (120 fs, 1 μJ/pulse), obtained from the idler output of the NIR OPA. All these experiments utilized a 2 mm-path-length fused-silica sample cell; all samples were deoxygenated by three consecutive freeze-pump-thaw cycles prior to use. All transient spectra reported represent averages obtained over at least 4 scans with each scan consisting of 150-250 time points.

Excited State Extinction Coefficients. Precise calculation of excited-state extinction coefficients of the NIR $S_1 \rightarrow S_n$ transient absorption bands utilizing a similar treatment of the fs transient absorption data to that used in a previous work[1] was complicated in these oligomeric porphyrin species. In the previous work,[2] where the negative signature in the femtosecond transient absorption spectra was due only to bleaching of the ground-state absorption, ε_e could be reasonably estimated by multiplying the ratio $|\Delta Abs.@ \lambda(S_1 \rightarrow S_n)|/|\Delta Abs.@\lambda(S_0 \rightarrow S_1)|$ by $\varepsilon_g @ \lambda(S_0 \rightarrow S_1)$. (Often it was necessary to modify the $|\Delta Abs.@\lambda(S_0 \rightarrow S_1)|$ to include an estimated contribution to positive excited-state absorption at this wavelength; see reference 2 Supporting Information for more details). For these conjugated oligomeric porphyrin species, however, additional bleaching contributions in the region of the Q-state absorption manifold derive from stimulated emission from the excited singlet state. Decoupling these two contributions to the negative transient absorption at the necessary wavelengths is not possible without knowing the relative contributions of each component; the best that can be said about the molar absorptivity of the $S_1 \rightarrow S_n$ excited-state transition is that it is similar in scale to the ground-state $S_0 \rightarrow S_1$ absorption. That is, if $S_0 \rightarrow S_n$ absorption for **DDDDD** has an ε_g at the λ_{max} (842 nm) of 230,000 $M^{-1}cm^{-1}$, then it is reasonable to conclude that $\varepsilon_e @ \lambda_{max}(S_1 \rightarrow S_n)$ is $> 10^5$ $M^{-1}cm^{-1}$.

Time-correlated, Single-Photon-Counting (TCSPC) Spectroscopy. TCSPC spectroscopic measurements were performed at the Regional Laser and Biotechnology Laboratory (RLBL) at the University of Pennsylvania using an instrument (response function = 25 ps FWHM) described previously[3]; these data were analyzed using Lifetime (RLBL) and Globals Unlimited (LFD, University of Illinois) Programs.

Fluorescence Quantum Yield Determination. The fluorescence quantum yields ϕ_f^x of these species were determined by the reference method,[4] using the relation:

$$\phi_f^x = \frac{A_s n_x^2 \int F_x}{A_x n_s^2 \int F_s} \phi_f^s \qquad \text{(S1)}$$

where $\int F_x$ and $\int F_s$ are the respective, total integrated fluorescence intensities of the unknown and emission standard, A_x and A_s are the corresponding wavelength-specific absorbances of the unknown and standard, respectively, and ϕ_f^s is the accepted

fluorescence quantum yield value for the standard chromophore. The quantity $(n_x/n_s)^2$ represents the solvent refractive index correction. The concentrations of all samples were adjusted such that their absorbance was between 0.005 and 0.04 at the excitation wavelength to minimize complications due to reabsorption effects. Fluorescence spectra obtained for the (porphinato)metal complexes, as well as the chromophores used as emission standards, were corrected to account for the wavelength-dependent efficiency of the detection system which was determined using the spectral output of a calibrated light source. All samples were degassed via purging with a stream of argon gas for ten minutes. Secondary corrections to the emission spectra used to determine ϕ_F (such as energy-dependent intensity corrections necessitated by the variable band pass/constant wavelength resolution data acquisition mode of the grating monochromator) were performed as outlined by Fery-Forgues.[4] Quantum yields were determined using free-base tetraphenylporphyrin ($\phi_F = 0.13$ in benzene[5]) as a standard benchmark. The standard error in quantum yields determined by this method is typically taken as ± 10% of the reported value.[4] The ϕ_F entries correspond to the average of values obtained from at least six independent measurements; corresponding standard deviations from the mean are also listed in Table 1 in parentheses.

Strickler-Berg Calculations of Radiative Rate Constants. Radiative rate constants, k_r, and corresponding intrinsic (natural) lifetimes, τ_o, were calculated by the Strickler-Berg[6] equation:

$$k_r = \frac{1}{\tau_0} = 2.88 \times 10^{-9} n^2 \left\langle \overline{\nu}_f^{-3} \right\rangle_{Av}^{-1} \frac{g_\ell}{g_u} \int \varepsilon d \ln \overline{\nu} \qquad \text{(S2)}$$

Where n is the solvent index of refraction, g_ℓ and g_u are the degeneracies of the emitting- and ground-states, respectively, ε is the extinction coefficient of the respective ground-state absorption band in wavenumbers, and k_r is the intrinsic (natural) radiative rate constant. The term $\left\langle \overline{\nu}_f^{-3} \right\rangle_{Av}^{-1}$ is given by the expression:

$$\left\langle \overline{\nu}_f^{-3} \right\rangle_{Av}^{-1} = \frac{\int I(\overline{\nu}) d\overline{\nu}}{\int \overline{\nu}^{-3} I(\overline{\nu}) d\overline{\nu}} \qquad \text{(S3)}$$

Here, I is the intensity of the fluorescence spectrum, measured in terms of relative numbers of quanta at each energy (frequency). Intermediate values for the calculation are

found in table S2. Note that the radiative rate constant is dependent on the emission frequency; however, the effect for this series (as illustrated by the data in Table S1) is minor compared to the dependency of the rate constant on the absorption band integrated oscillator strengths.

The observed fluorescence lifetime (τ_{es} or τ_f, when determined via transient absorption or time-resolved fluorescence, respectively) can be obtained with the relation: $\tau_{es} = \tau_o * \phi_f$, where ϕ_f is the quantum yield of fluorescence.

Corresponding nonradiative rate constants (including contributions due to intersystem crossing (k_{isc}) and internal conversion (k_{ic})) can also be derived by the following expression:

$$k_{nr} = k_r\left(\frac{1}{\phi_f} - 1\right) \qquad \text{(S4)}$$

All of these calculated values appear in Table 1 in the main text or Table S1 in this Supporting Information section. Plots of these values versus number of constituent porphyrin units appear in the Supporting Information figures. Similar calculations were performed on benchmarks [5,10,15,20-tetraphenylporphinato]zinc(II) (**TPPZn)** and [5,15-bis(trimethylsilylethynyl)-10,20-bis(3,5-bis(9-methoxy-1,4,7-trioxanonyl)phenyl)porphinato]zinc(II) (**E-D-E**) for comparison.

Additional Discussion of Trends in Table 1 Data. Table 1/Table S1 includes the fluorescence quantum yields (ϕ_F), experimentally determined excited-state lifetimes (τ_{es} or τ_F), and Strickler-Berg calculated radiative lifetimes (τ_0) of bis-, tris- and pentakis-ethyne-bridged (porphinato)zinc(II) arrays (**PZn$_n$**). In the main text of this manuscript, it was stated that the trends in ϕ_F and τ_{es} can be rationalized in terms of the magnitudes of the radiative (k_r, $(\tau_0)^{-1}$) and nonradiative (k_{nr}) rate constants, and the comparison of **DAD** and **DADAD** was cited as an example. Here, the additional example of **DD** vs. **DDDDD** is presented in detail.

Experimentally, **DD** and **DDDDD** possess similar ϕ_F (16% and 14%, respectively), despite having emission energies that are over 2740 cm^{-1} apart, an observation which is contrary to the classical predictions of the energy gap law. The explanation for this effect involves three points, which are illustrative of a more general

approach to understanding the trends underlying the data in Table 1. A simple Jablonski diagram (Scheme S1) is provided to help illustrate these points.

First: the Strickler-Berg relationship predicts that the radiative rate constant of **DDDDD** is 5-fold larger than that of **DD**, because the former possesses a lowest-energy ground-state absorption band integrated oscillator strength (*f*) that is significantly larger than that of the latter (Tables S1 and S2). There is an additional effect which involves a dependency of k_r on the emission frequency (*vide supra*), but Table S2 shows that this effect is relatively minor in comparison. Thus a Strickler-Berg analysis predicts that, due mostly to its larger k_r, **DDDDD** should, all other things being equal, possess the larger ϕ_F.

Second: the ϕ_F is also dependent on the k_{nr} (*vide supra*). In most organic chromophores, as has been noted already, the energy gap law predicts that for two similar species, the compound that possesses the smaller optical band gap will also have the smaller ϕ_F, because the rate constant of internal conversion (k_{ic}) to the ground electronic surface is directly dependent on the Franck-Condon overlap of the ground- and excited-state vibrational wavefunctions, which is larger for smaller S_0-S_1 energy gaps. Thus, an energy-gap law analysis predicts that, due to its larger k_{ic}, **DDDDD** should possess the smaller ϕ_F. It is noteworthy that in most examples of low band-gap materials, k_{ic} is the most important factor in determining the magnitude of ϕ_F, with k_r playing only a minor role.[7-9]

Third: as shown below in the section on the ultrafast excited-state dynamics, as the number of constituent monomeric units increases, there is an increasingly large barrier to intersystem crossing. In fact, in the case of **DDDDD**, the intersystem crossing rate constant, k_{isc}, is very small relative to k_{ic} and k_r. k_{isc} and k_{ic} are the two major contributors to the total nonradiative decay rate (k_{nr}) via the expression

$$k_{nr} \sim k_{isc} + k_{ic} \qquad \text{(S5)}$$

Thus it is shown that, because k_{ic}(**DDDDD**) > k_{ic} (**DD**) but k_{isc}(**DDDDD**) < k_{isc}(**DD**), the overall effect of the intersystem crossing term is to temper the precipitous drop in ϕ_F as a function of the **PZn$_n$** optical band gap that is expected from classical energy gap law considerations. It should be stressed that the excited-state lifetimes reported in Table 1 indicate that the k_{ic} term is still the dominant effect (e.g., τ_{es}(**DDDDD**) ~ 450 ps vs. τ_{es}(**DD**) ~ 1.09 ns), but the loss of intersystem crossing as a viable decay channel as well

as the larger radiative rate constant that is exhibited by **DDDDD** makes ϕ_F large in the largest members of this unique series of fluorophores despite their low emission energies.

As shown in Table S1, the observed and calculated fluorescence quantum yields are, considering the simplicity of the Strickler-Berg approach, exceptional in their agreement. Strickler and Berg require that two conditions be met for their treatment to be valid: "First that the [ground-state absorption] band be strong, and second that there not be too large a change on configuration in the excited state".[6] Of specific note is the reported difficulty of the method in predicting k_r for systems which are known to undergo modest excited-state structural relaxation processes. As shown below, all the fluorophores studied herein do exhibit such processes, which may introduce some error into the Strickler-Berg calculations. **DD** and **DA** are the compounds whose calculated ϕ_F values exhibit the largest deviations from experimental values, which is due to their weaker ground-state absorption bands, as the Strickler-Berg method is also known to be less accurate for these species. Nonetheless, the calculated ϕ_F values are within the range of errors generally reported in the literature.[6]

Ultrafast Dynamics of DD and DA. The ultrafast dynamics of **DD** and **DA** have been previously reported.[10] In this prior work, femtosecond transient hole burning spectroscopy was used to investigate the isotropic and anisotropic excited-state dynamics following photoexcitation of these chromophores. It was found that the supermolecular delocalization of the excited-state resulted in an *intense* ($\varepsilon \geq 3 \times 10^5$ M^{-1} cm^{-1}) $S_1 \rightarrow S_n$ near-infrared transition (**DD**: λ_{max} = 980 nm; **DA**: λ_{max} = 953 nm).[10] The time-dependent evolution of the $S_1 \rightarrow S_n$ manifold was found to be sensitive to the electronic symmetry of the delocalized excited-state. In the electronically asymmetric **DA**, solvent dipole reorientation was found to be strongly coupled to interporphyrin torsional angle relaxation dynamics, which resulted in a time-dependent augmentation of the excited-state dipole moment (μ_{ge}) and a marked decrease over a <2 ps timescale of the excited-state $S_1 \rightarrow S_n$ and steady state fluorescence ($S_1 \rightarrow S_0$) transition moments. In contrast, electronically symmetric **DD** displayed little evolution of the excited-state spectra on solvent response timescales. **DDD**, **DAD**, **DDDDD**, and **DADAD** are expected to behave similarly to **DD**, as these species possess no ground-state dipole moment[1]; however the increased size of **DDD**, **DAD**, **DDDDD** and **DADAD** leads to both greater spectral

heterogeneity relative to the **DD** and **DA** benchmarks studied previously, and correspondingly more complicated excited-state dynamics. As the systems get larger, the molecules explore a vast conformational space which modulates the extent to which these **PZn$_n$** structures are conjugated: due to the low barrier to rotation about the ethyne bridge, each *meso*-to-*meso* ethyne linkage is characterized by a wide distribution of PZn-PZn torsional angle. Consequently quantitative analysis of these independent processes becomes difficult as oligomeric size increases. Therefore, the excited-state dynamics of the smaller systems **DDD** and **DAD**, are discussed henceforth in some detail, but **DDDDD** and **DADAD** are discussed only qualitatively.

Ultrafast Transient Absorption Spectra of DDD. The fs and ps timescale spectra obtained for **DDD** (Figure S4A), excited at 690 nm, display four pronounced features: (i) a high oscillator strength bleach in the B-band ($S_0 \rightarrow S_2$) region, (ii) a transient absorption between the Soret and x-polarized Q states in the ~500-650 nm spectral domain, (iii) a bleach in the Q-band region that partly overlaps with the stimulated emission signal, and (iv) an intense $S_1 \rightarrow S_n$ NIR transient absorption. The first three features are typical of transient spectra of porphryin-based chromophores; the fourth feature is discussed in the primary text of this manuscript. At long delay times (t_{delay} ~ 6 ns), a new transition at 1210 nm can be seen that corresponds to the $T_1 \rightarrow T_n$ triplet state absorption. This feature persists beyond the time-domain of this instrument. The energy separation between the excited-state singlet and triplet absorptions is determined to be 530 cm^{-1}, which is slightly larger than that determined for **DD** (~400 cm^{-1}).[10]

Polarized pump-probe spectroscopy (data not shown) reveals that the **DDD** NIR transient absorption bands exhibit initial anisotropy values of 0.4, indicating that the $S_0 \rightarrow S_1$ and $S_1 \rightarrow S_n$ (S_n being a higher delocalized singlet excited-state) transitions are mutually parallel and directed along the highly conjugated axis defined by the ethyne bridges. This result is similar to that seen in the analogous studies of **DD**[10] as well as that found for the other compounds in this series, and is in contrast to circular absorbers such as conventional (porphinato)metal monomers, which possess anisotropy values of ~0.1.

One feature in the spectra shown in Figure S4A that is *not* manifested in the NIR transient absorption spectra of **DD** is the existence of a second peak maximum (λ ~ 1000

nm) on the high-energy side of the intense 1120 nm NIR transient absorption band. The higher energy transition (1000 nm) occurs nearly at the same energy as the **DD** $S_1 \rightarrow S_n$ absorption (~980 nm); it is thus proposed that this transition results from a population of **DDD** electronically excited-states in which excitation is confined predominantly to two adjacent porphyrin moieties; such "**DD**-like" structural conformations would occur when two adjacent porphyrins are nearly coplanar and the third porphyrin is rotated to a significant degree out of this plane. Such **DDD** partially-localized excited-states would exhibit spectroscopic features similar to the **DD** excited-state.

Because of the ground-state conformational heterogeneity, a spectrally narrow Q_x-state excitation pulse burns a hole within the conformeric distribution; spectral diffusion (i.e., equilibration of the relatively structurally homogeneous initially-prepared excited-state population) plays a key role in the time-dependent evolution of the transient spectrum. Optical pumping on the blue side of the **DDD** Q_x manifold (λ_{ex} = 690 nm, Figure S5A) excites a distribution of ground-state conformers featuring relatively large torsional angles between the respective porphyrin least-squares planes. Figure S5A shows that the NIR transient absorption λ_{max} red-shifts (9 nm, ~70 cm^{-1}) and intensifies (~17%) during the first ~100 ps following excitation. On this same time scale, the 1000 nm transition (assigned above as a "**DD**-like" state) λ_{max} decreases in intensity by ~50%. At time delays greater than 100 ps, the entire NIR transient spectrum decays, but the 1000 nm transition continues to decay at a faster rate than the 1250 nm transition. On the same time-scale, the Q-state bleaching signature also slightly red-shifts.

Excitation on the high-energy side of the **DDD** Q_x-state manifold (λ_{exc} = 690 nm) initiates spectral diffusion of an excited-state conformeric population having less than optimal PZn-PZn conjugation towards structures having smaller average interporphyryl angles (Figure S5A). Such an equilibration process results in a red-shift of both the ground-state bleach and stimulated emission signals during the fast time domain (t < 100 ps), as well as a red-shift of the NIR $S_1 \rightarrow S_n$ transient absorption band. Additionally, as more planar **DDD** populations possess larger transition moments owing to enhanced PZn-PZn conjugation, the NIR $S_1 \rightarrow S_n$ band is expected to increase in intensity as it red shifts. These findings are consistent with what was reported for **DD**[10] excited-state dynamics. However, the case of **DDD** is complicated by the existence of additional transitions in the

$S_1 \rightarrow S_n$ manifold. If the additional transition ($\lambda \sim 1000$ nm) is assigned to **DD**-like excited-state species, then spectral diffusion following excitation on the high-energy side of the Q_x-state absorption manifold (which produces an initial excited-state population consisting largely of **DD**-like conformers) should reduce the intensity of this transition, which is seen in Figure S5A.

Figure S5B shows an analogous experiment to the one shown in Figure S5A, except λ_{exc} is 775 nm, which falls nearly in the center of the Q-state absorption band. At this excitation wavelength, a population of conformers is excited that possesses augmented ground-state conjugation (decreased average porphyrin-porphyrin interplanar torsional angles relative to that probed with $\lambda_{exc} = 690$ nm). In the Q_x-state bleaching region a slight broadening of the bleach signature and stimulated emission signal is manifested during the course of spectral diffusion. In the NIR energy regime, only a subtle (~ 1 nm) red-shift occurs after excitation at 775 nm (Figure S5B). Furthermore, immediately after 775 nm excitation ($\tau \sim 500$ fs), the 1000 nm transition is weak (ΔAbs. (λ = 1000 nm) / ΔAbs. (λ = 1120 nm) = 0.10) in intensity compared to its initial intensity after 690 nm excitation (ΔAbs.(λ = 1000 nm) / ΔAbs. (λ = 1120 nm) = 0.21). Additionally, the 1000 nm transition exhibits none of the sub-100 ps dynamics that was seen with the 690 nm excitation experiment. This result supports the assignment of the 1000 nm transition to a conformational distribution that gives rise to a "**DD**-like" excited-state structure. A greater initial population of these higher-energy absorbing conformers would be produced for $\lambda_{exc} = 690$ nm, with time dependent spectral diffusion reducing its population. In contrast, 775 nm excitation generates a smaller initial excited-state population of these higher-energy-absorbing conformers; as a result there is very little spectral diffusion towards more planar conformers with time after excitation at this wavelength. Note that after spectral diffusion time scales (t = 100 ps), the NIR transient absorption spectra following excitation at both 690 nm and 775 nm are nearly identical, indicating conformational equilibration has occurred.

Global exponential fitting of the **DDD** NIR spectral dynamics ($\lambda_{exc} = 690$ nm) evinces five relaxation processes with the following lifetimes: 500 fs, 1.8 ps, 70 ps, 130 ps and 1.24 ns. The 1.24 ns decay is assigned to the intrinsic excited-state lifetime and agrees well with the fluorescence lifetime determined by time-correlated single photon-

counting spectroscopy (see text). By analogy to the **DD** assignments,[10] the two fastest components can be assigned to inertial solvent polarization and reorientation, respectively, as they are very close to the THF solvent relaxation times.[11] The other components (70 ps and 130 ps) are assigned to spectral diffusion. The spectral diffusion time for **DDD** is longer than that determined for **DD** (30 ps)[10] due to its augmented size and the fact that the central porphyrin unit possesses solubilizing polyethylene glycol groups that increase the average timescales for PZn rotation and libration about the ethyne bridge. It should be noted that the 70 ps and 130 ps processes should not necessarily be viewed as separate processes and probably represent the weighted averages of several higher order exponential decay components; this is because spectral diffusion in **DDD** is expected to be more complex (and multiexponential) relative to that observed for **DD** due to extra degrees of rotational degrees of freedom deriving from the additional porphyrin unit. Fitting the 775 nm excitation data yields similar lifetime values for the observed relaxation processes.

Ultrafast Transient Absorption Spectra of DAD. As noted above, electronically excited **DDD** and **DAD** are expected to display similar dynamics since both species possess electronically symmetric ground states.[1] Indeed, this appears to be the case from a simple inspection of steady-state emission and absorption spectra (main text).

Figure S4B depicts the early (300 fs) and late (6 ns) transient absorption spectra of **DAD** in THF, excited at 690 nm, which is on the high energy side of the **DAD** Q_x-state absorption band. **DAD** shows the same general transient-absorption spectroscopic features of **DD** and **DDD** discussed above. The intense $S_1 \rightarrow S_n$ NIR transient absorption band is blue-shifted (50 nm, 420 cm^{-1}) with respect to that observed for **DDD**, due to the σ–electron withdrawing 10-20-perfluoroalkyl groups of the **DAD** central PZn unit, which uniformly lowers the energy of the **DAD** frontier orbitals relative to **DDD**.[1]

The spectra shown in Figure S4B manifest several differences relative to analogous spectra evinced for **DDD** (S4A), the most noticeable of which is the spectral width of the NIR transition. In the **DDD** spectrum, this transition is narrow and centered at 1120 nm (FWHM ~ 740 cm^{-1}) with a well-resolved, high energy shoulder (λ ~ 1000 nm). In the **DAD** excited-state NIR absorptive manifold, there are both high (λ ~ 944 nm) and low (λ ~ 1184 nm) energy secondary transitions; the high energy counterpart is

mostly overlapped by the intense 1070 nm band. These transitions give rise to a broad absorptive envelope (FWHM = 1585 cm^{-1}). Analogous to the 1000 nm transition in **DDD**, the 944 nm band is assigned to a transition that derives from a **DA**-like state, where two adjacent PZn units are relatively coplanar, with the third PZn component lying at a larger torsional angle with respect to the **DA** plane. The larger spectral breadth of the **DAD** absorption features and the corresponding lowest energy absorption is likely due to augmented charge-resonance in **DAD** conformers possessing small interporphyryl torsional angles.

The other noticeable difference between **DAD** and **DDD** in Figure S4B is evident in the late time (~6 ns) spectrum. This spectrum is dominated by excited triplet state absorption and it is readily apparent that there are two absorption maxima (977 nm and 1315 nm). This is in contrast to **DDD** where there is a single triplet absorption at ~1200 nm. The difference in energy between the two triplet transitions of **DAD** is too large (2630 cm^{-1}) to be vibrational in origin and these spectroscopic features may be due to the presence of T_1 states localized on either the A and D units of **DAD**, or may correspond to ($T_1 \rightarrow T_n$) and ($T_1 \rightarrow T_{n+1}$) triplet-state absorptions, respectively.

Ultrafast transient spectra recorded for **DAD** (Figure S6) exhibit subtly different time-dependent changes from those exhibited in the analogous **DDD** spectra (Figure S5A). Shown in Figure S6A are the transient spectra at several time delays following excitation at 690 nm, which lies on the high-energy side of the Q_x-transition. During the first 5 ps following photoexcitation where solvent relaxation dynamics dominate, there is a slight decrease in intensity of most over the NIR spectral region; this decrease in intensity is much more pronounced for the high energy (944 nm) transition, and contrasts the **DDD** excited-state dynamics highlighted in Figure S5. That solvent relaxation causes a rapid decrease in the intensity of the **DA**-like excited-state absorption in the **DAD** excited-state absorption spectrum but not in the intensity of the **DD**-like excited-state absorption evident in the **DDD** excited-state absorption manifold (λ_{max} = 1000 nm, Figure S5) is not surprising. Optical transitions deriving from populations of electronically-excited **DA**-like conformers resulting from the high-energy Q_x-state excitation of **DAD**, would be expected to have electronically asymmetric excited-state wave-functions similar to that exhibited by ^{1}**(DA)***; such **DAD** excited-state conformeric populations

would be expected to exhibit solvent-relaxation dynamics akin to those exhibited by electronically asymmetric ^{1}**(DA)*** (vide supra). Conversely, optical transitions deriving from **DAD** conformeric populations having more delocalized excited-states (λ_{max} = 1070 nm) would evince only modest evolution of the 1070 nm transient absorption band, due to the fact that these relaxation dynamics do not drive formation of excited-states having increased polarization.

Spectral evolution following photoexcitation of **DAD** on timescales longer than those typically associated with solvent dynamical processes (i.e., $\tau > 5$ ps) are qualitatively similar to those described in the **DDD** experiment (vide supra); as in **DDD**, such processes are generally due to spectral diffusion of excited-state conformations differing primarily with respect to the average magnitude of their respective PZn-PZn interporphyrin torsional angle. The **DAD** transient absorption spectra obtained after photoexcitation at 775 nm (Figure S6B) show dynamics similar results to those described for **DDD** (Figure S5B). Global exponential fitting of the **DAD** NIR transient spectral dynamics at both excitation wavelengths evinces five relaxation processes with the following lifetimes: 350 fs, 2 ps, 50 ps, 195 ps and 1.5 ns. The assignments of these processes are identical to those described for **DDD** (vide supra).

Ultrafast Transient Absorption Spectra of DDDDD and DADAD. Figures S4C and D depict the early (620 fs) and late (5.5 ns) spectra of **DDDDD** and **DADAD**, respectively, excited at 775 nm, which is on the high energy side of the respective Q-state electronic absorption manifolds of these oligomers. Both sets of early time spectra display broad NIR $S_1 \rightarrow S_n$ absorptions, with λ_{max} = 1326 nm (7634 cm^{-1}) for **DDDDD** and λ_{max} =1194 nm (8375 cm^{-1}) for **DADAD**. In **DDDDD** (Figure S4C) this NIR transition is significantly red-shifted (1327 cm^{-1} and 2561 cm^{-1}, respectively) compared to **DDD** and **DD**; likewise the analogous feature in **DADAD** is significantly red-shifted (1100 cm^{-1} and 2100 cm^{-1}, respectively) compared to **DAD** and **DA**.

While electronically-excited **DD** and **DDD** possess NIR transient absorption bands that are relatively narrow (FWHM = 656 cm^{-1} and 750 cm^{-1}, respectively), electronically-excited **DDDDD** has a NIR transition manifold that is significantly broadened (FWHM = 1982 cm^{-1}), with two distinct absorption maxima that are almost equal in intensity (with λ_{max} at 1180 nm and 1326 nm, respectively). The fact that the

DDDDD excited-state spectra feature a NIR absorptive manifold broader than either **DD** or **DDD** is consistent with the greater degree of interporphyryl torsional heterogeneity possible in a **PZn$_5$** oligomer. Whereas the 1326 nm **DDDDD** near-infrared transition is assignable to an S_1 excited state that is delocalized over all five porphyrins, the 1180 nm transition may owe its genesis to (by analogy to the case of **DDD**) **DDD**-like or **DDDD**-like excited-state conformations. That these less-delocalized states are major contributors to the ensemble-average transient spectra shown in Figure S4C should not be surprising considering that the high energy 775 nm excitation wavelength selectively probes **DDDDD** ground-state populations having mean interporphyryl torsional angles that are large with respect to the ensemble average. A large spectral breadth as well as multiple peak maxima in the NIR $S_1 \rightarrow S_n$ transition manifold is also exhibited by **DADAD** (Figure S4D).

The other noticeable difference between the transient spectra of **DDDDD** and **DADAD** and the analogous spectra for the tris- and bis(porphinato)zinc(II) arrays in Figure S4 can be seen in the spectra at long time delays ($t_{delay} \sim 5$ ns), which are dominated by $T_1 \rightarrow T_n$ absorptions. Interestingly, Figures S4C and D show a conspicuous lack of any appreciable $T_1 \rightarrow T_n$ absorption feature at 5.5 ns time delay in the transient spectra of both **DDDDD** and **DADAD**; i.e. the intersystem crossing (ISC) pathway is increasingly inhibited with increasing conjugation length.[12] This finding is in agreement with electron paramagnetic resonance (EPR) studies[13-15] which suggest a significant barrier to ISC in these conjugated PZn oligomers due to the disparate spatial extents of the singlet (delocalized) and triplet (localized) excited-state wavefunctions. Increasing oligomeric size thus results in increasingly diminished Franck-Condon overlap between the S_1 and T_1 state wavefunctions. Since **DDDDD** and **DADAD** (Figure S4C and D) exhibit no measurable T_1-state yield following photoexcitation at ambient temperature, this suggests that ISC no longer contributes to excited singlet-state deactivation. Diminished quantum yields anticipated by the energy gap law due to the enhanced S_1-S_0 vibrational wavefunction overlap that occurs with decreasing S_1-S_0 energy separations as conjugation length increases are largely counteracted by a concomitant reduction in the magnitude of k_{isc}. This effect plays a prominent role in determining the large NIR ϕ_f values observed for **DDD**, **DAD**, **DDDDD** and **DADAD** and points to engineering

disparate S_1 and T_1-state delocalization lengths as a viable approach to engineering low-energy high quantum-yield fluorophores.

Excited-state relaxation dynamics of **DDDDD** and **DADAD** were analyzed in a similar fashion to that described for **DDD** and **DAD**; these dynamics bear many similarities to those described above for **DDD** and **DAD** excited states. Transient spectra at several time delays are shown in Figure S7 and S8 for **DDDDD** and **DADAD**, respectively. Briefly: both pentakis(porphinato)zinc(II) arrays manifest very little global solvent-dependent relaxation dynamics, in agreement with the electronically-symmetric nature of their respective ground-states.[1] The exception to this generalization can be seen is in the 900-950 nm region of the **DADAD** $S_1 \rightarrow S_n$ transient absorption manifold, which would be expected to be dominated by absorption of asymmetric excited electronic states resembling that described for **DA**[10]; this region of the of $S_1 \rightarrow S_n$ transient absorption manifold undergoes fast deactivation on the solvent dipole reorientation timescale, analogous to what was seen for **DA**.[10] Not surprisingly, $S_1 \rightarrow S_n$ transitions that correspond to **DADAD** conformeric populations that give rise to both the **DAD**-like ($\sim$1000 nm $< \lambda <$ 1100 nm) and globally delocalized **DADAD**-like (λ_{max} = 1206 nm) excited-states exhibit only slight intensity changes over solvent relaxation time-scales, owing to the symmetric nature of their respective excited-states.

Global fitting of the NIR decay dynamics evince processes having similar magnitudes and amplitudes to those exhibited by the tris(porphinato)zinc(II) arrays; the excited-state spectral diffusion processes of **DDDDD** and **DADAD**, however, are more highly multiexponential than that for their trimeric analogues due to augmented structural heterogeneity.

References:

(1) Susumu, K.; Therien, M. J. *J. Am. Chem. Soc.* **2002**, *124*, 8550-8552.

(2) Duncan, T. V.; Rubtsov, I. V.; Uyeda, H. T.; Therien, M. J. *J. Am. Chem. Soc.* **2004**, *126*, 9474-9475.

(3) Holtom, G. R. *SPIE Proc.* **1990**, *1204*, 2-12.

(4) Fery-Forgues, S.; Lavabre, D. *J. Chem. Edu.* **1999**, *76*, 1260-1264.

(5) Quimby, D. J.; Longo, F. R. *J. Am. Chem. Soc.* **1975**, *97*, 5111-5117.

(6) Strickler, S. J.; Berg, R. A. *J. Chem. Phys.* **1962**, *37*, 814-820.

(7) Englman, R.; Jortner, J. *Mol. Phys.* **1970**, *18*, 145-164.

(8) Caspar, J. V.; Kober, E. M.; Sullivan, B. P.; Meyer, T. J. *J. Am. Chem. Soc.* **1982**, *104*, 630-632.

(9) Caspar, J. V.; Meyer, T. J. *J. Phys. Chem.* **1983**, *87*, 952-957.

(10) Rubtsov, I. V.; Susumu, K.; Rubtsov, G. I.; Therien, M. J. *J. Am. Chem. Soc.* **2003**, *125*, 2687-2696.

(11) Reynolds, L.; Gardecki, J. A.; Frankland, S. J. V.; Horng, M. L.; Maroncelli, M. *J. Phys. Chem.* **1996**, *100*, 10337-10354.

(12) While it is possible that the **DDDDD** $T_1 \rightarrow T_n$ absorption band could occur with λ_{max} > 1400 nm, the lack of any bleaching of the ground-state absorption bands at t_{delay} > 1 ns confirms the lack of any appreciable T_1-state population.

(13) Angiolillo, P. J.; Lin, V. S. Y.; Vanderkooi, J. M.; Therien, M. J. *J. Am. Chem. Soc.* **1995**, *117*, 12514-12527.

(14) Shediac, R.; Gray, M. H. B.; Uyeda, H. T.; Johnson, R. C.; Hupp, J. T.; Angiolillo, P. J.; Therien, M. J. *J. Am. Chem. Soc.* **2000**, *122*, 7017-7033.

(15) Angiolillo, P. J.; Uyeda, H. T.; Duncan, T. V.; Therien, M. J. *J. Phys. Chem. B* **2004**, *108*, 11893-11903.

(16) Ohno, O.; Kaizu, Y.; Kobayashi, H. *J. Chem. Phys.* **1985**, *82*, 1779-1787.

Scheme Captions:

S1. Jablonski diagram showing the most important factors which influence the observed/calculated fluorescence quantum yield. The blue arrow represents absorption from S_0 to S_1 state with integrated oscillator strength, *f*. The solid red arrow represents fluorescence; dashed red arrows represent nonradiative relaxation pathways. Processes relating to the relaxation of the T_1 state to the S_0 ground state are omitted for clarity, as they do not contribute to the fluorescence quantum yield.

Table Captions:

S1. Spectroscopic Parameters of Oligomers **DD, DA, DDD, DAD, DDDDD** and **DADAD,** determined in THF solvent**.**

S2. Intermediate values from the Strickler-Berg calculations.

Figure Captions.

S1. Plot of calculated Strickler-Berg radiative rate constants as a function of number of porphyrin units.

S2. Plot of calculated and observed fluorescence quantum yields as a function of number of porphyrin units.

S3. Plot of calculated nonradiatve rate constants as a function of number of porphyrin units deriving from calculated Strickler-Berg radiative rate constants and calculated fluorescence quantum yields.

S4. Magic angle transient absorption spectra of (A) **DDD**, (B) **DAD**, (C) **DDDDD** and (D) **DADAD** in tetrahydrofuran solvent, measured at time delays of 300 fs (solid black line) and 6 ns (solid blue line). The excitation wavelengths were 690 nm (A and B) and 775 nm (C and D). The horizontal dotted line in each figure represents a Δabs. of 0.

S5. DDD transient absorption spectra determined at magic angle polarization in tetrahydrofuran; delay times = 500 fs, 10.5 ps, 103 ps, 1 ns, 2 ns, and 6 ns: (A) λ_{ex} = 690 nm and (B) λ_{ex} = 775 nm. Scaled steady-state absorption (dotted blue line) and fluorescence (dotted red line) spectra are displayed for comparative purposes. Thick arrows denote spectral changes that occur with increasing time.

S6. **DAD** transient absorption spectra determined at magic angle polarization in tetrahydrofuran; delay times = 515 fs, 10 ps, 107 ps, 1.1 ns, 2.2 ns, and 5.8 ns: (A) λ_{ex} = 690 nm and (B) λ_{ex} = 775 nm. Scaled steady-state absorption (dotted blue line) and

fluorescence (dotted red line) spectra are displayed for comparative purposes. Thick arrows denote spectral changes associated with spectral diffusion that occur with increasing time.

S7. DDDDD transient absorption spectra determined at magic angle polarization in tetrahydrofuran; delay times = 500 fs, 10.5 ps, 103 ps, 1 ns, 2 ns, and 6 ns; λ_{ex} = 775 nm. Scaled steady-state absorption (dotted blue line) and fluorescence (dotted red line) spectra are displayed for comparative purposes. Thick arrows denote spectral changes that occur with increasing time.

S8. **DADAD** transient absorption spectra determined at magic angle polarization in tetrahydrofuran; delay times = 515 fs, 10 ps, 107 ps, 1.1 ns, 2.2 ns, and 5.8 ns: (A) λ_{ex} = 775 nm. Scaled steady-state absorption (dotted blue line) and fluorescence (dotted red line) spectra are displayed for comparative purposes. Thick arrows denote spectral changes associated with spectral diffusion that occur with increasing time.

Table S1. Spectroscopic Parameters of Oligomers **DD, DA, DDD, DAD, DDDDD** and **DADAD,** determined in THF solvent**.**

	$\Phi_{f,\,obs}$	$\Phi_{f,calc}$, (FTAS)[a]	$\Phi_{f,calc}$, (TCSPC)[b]	τ_{es} (FTAS)[c] [ns]	τ_f (TCSPC)[c] [ns]	$k_{r,calc}$ [x10^7 s^{-1}]	k_{nr} (FTAS)[d] [x10^7 s^{-1}]	k_{nr} (TCSPC)[e] [x10^7 s^{-1}]	k_f, *calc*[j] [x10^{7}s^{-1}]	τ_{es}, *calc*[j] [ns]
ZnTPP[f]	0.033[g]		0.031		2.0[h]	1.81		48.1	54.9	1.82
E-D-E	0.069		0.043		1.73	2.48		55.3	35.9	2.78
DD	0.16	0.06	0.062	1.12	1.09	5.72	83.6	86.4	35.7	2.80
DDD	0.22	0.16	0.154	1.2	1.13	13.65	69.7	75.1	62.0	1.61
DDDDD	0.14	0.15	0.126	0.54	0.45[i]	28.02	158.9	209.5	20.0	0.50
DA	0.063	0.04	0.033	1.17	0.896	3.64	81.8	108.0	57.8	1.73
DAD	0.17	0.14	0.112	1.4	1.11	10.06	61.4	79.8	59.2	1.69
DADAD	0.19	0.16	0.134	0.85	0.695[i]	19.28	97.8	124.7	10.2	0.99

[a]Fluorescence quantum yield, calculated from the k_r (determined by Strickler-Berg analysis of fluorescence and absorption spectra) and by the excited-state lifetime determined by FTAS. Since the benchmarks **TPPZn** and **E-D-E** were not interrogated by FTAS, no calculation exists for these compounds. [b]Fluorescence quantum yield, calculated from the k_r determined by Strickler-Berg analysis of fluorescence and absorption spectra and by the excited-state lifetime determined by TCSPC spectroscopy. [c]Excited-state/fluorescence lifetime determined by FTAS or TCSPC spectroscopy, as indicated. [d]Nonradiative rate constant for excited-state decay, calculated from $\Phi_{f,calc}$, (FTAS) and τ_r (k_r^{-1}). [e]Nonradiative rate constant for excited-state decay, calculated from $\Phi_{f,calc}$, (TCSPC) and τ_r, the inverse of k_r. [f]Data for **TPPZn** was recorded in benzene solvent. Note that because the benchmark compounds TPPZn and E-D-E are included, some of the data columns from Table 1 in the text have been repeated. [g]This value was taken from reference 5. [h]This value was taken from the reference 16. [i]The excited-state lifetimes of the two pentameric complexes determined by TCSPC spectroscopy were highly multiexponential and varied slightly with excitation wavelength. The reported value represents an average of at least three separate measurements. [j]The fluorescence rate constant and corresponding excited-state lifetime, calculated from the experimental quantum yield and the calculated Strickler-Berg natural radiative rate constant, k_r.

Table S2. Intermediate values from the Strickler-Berg calculations.

Compound	$\int \varepsilon d\ln\bar{\nu}$ [$M^{-1}cm^{-2}$]	n^2	$\int I(\bar{\nu})d\bar{\nu}$ [cm^{-1}]	$\int \bar{\nu}^{-3} I(\bar{\nu})d\bar{\nu}$ [cm^{-4}]	g_ℓ / g_u	$\langle \bar{\nu}_f^{-3} \rangle_{Av}^{-1}$ [$x10^{12}$ cm^{-3}]
ZnTPP	1468	2.253001	1.24E+38	3.26E+25	**0.5**	3.8
E-D-E	1259	1.979649	1.18E+34	3.42E+21	**1**	3.45
DD	4748	1.979649	2.06E+38	9.73E+25	1	2.11
DA	3568	1.979649	5.21E+33	2.91E+21	1	1.79
DDD	14360	1.979649	1.22E+34	7.34E+21	1	1.67
DAD	10432	1.979649	1.36E+34	8.06E+21	1	1.69
DDDDD	37053	1.979649	4.86E+33	3.67E+21	1	1.33
DADAD	23179	1.979649	8.88E+33	6.09E+21	1	1.46

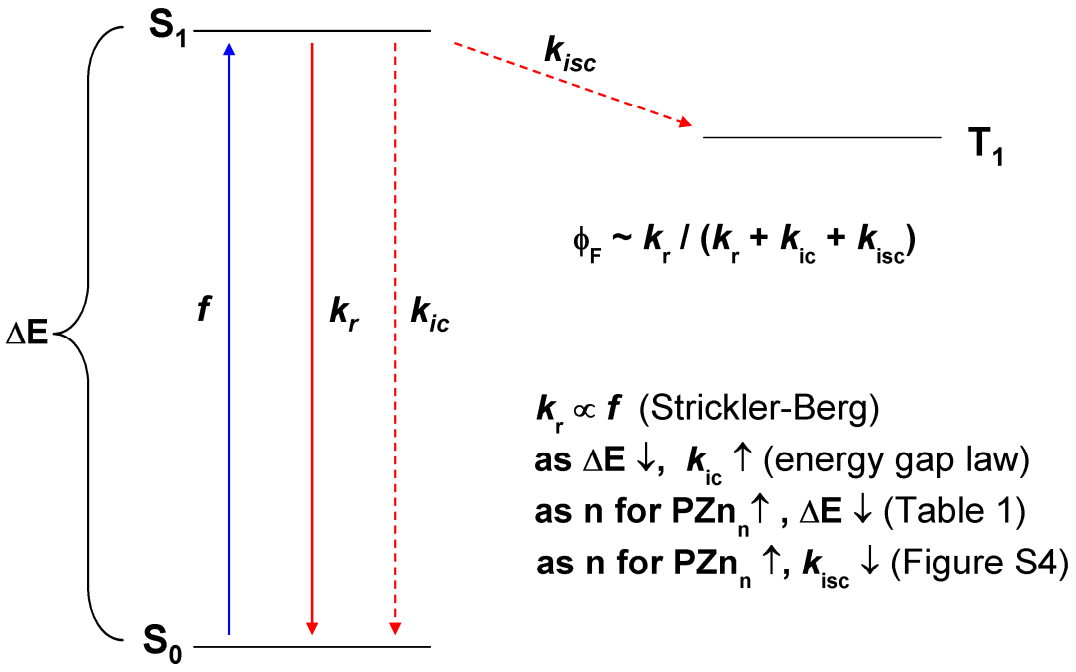

Scheme S1

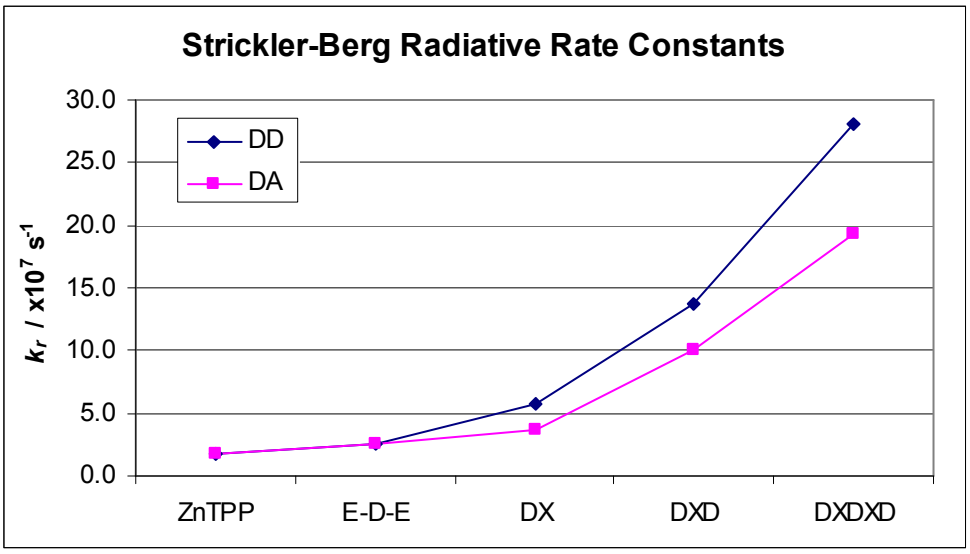
Strickler-Berg Radiative Rate Constants
30.0
25.0
20.0
15.0
10.0
5.0
0.0
k_r / x10^7 s^{-1}
DD
DA
ZnTPP
E-D-E
DX
DXD
DXDXD

Figure S1.

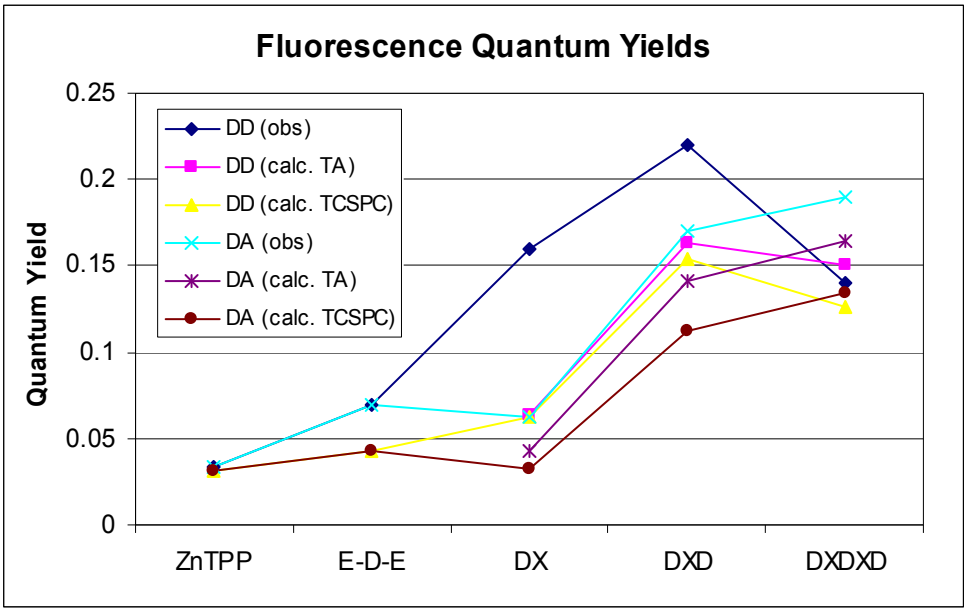

Figure S2

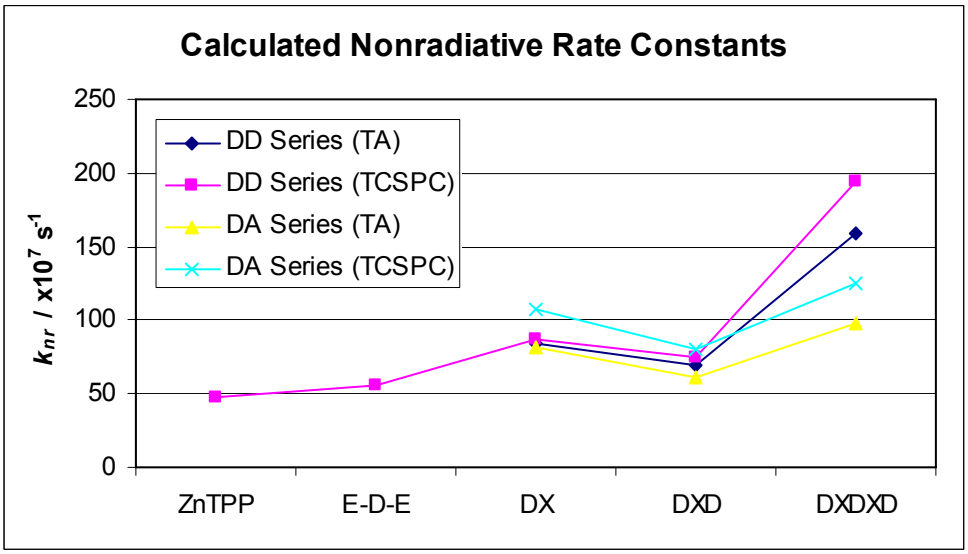

Figure S3

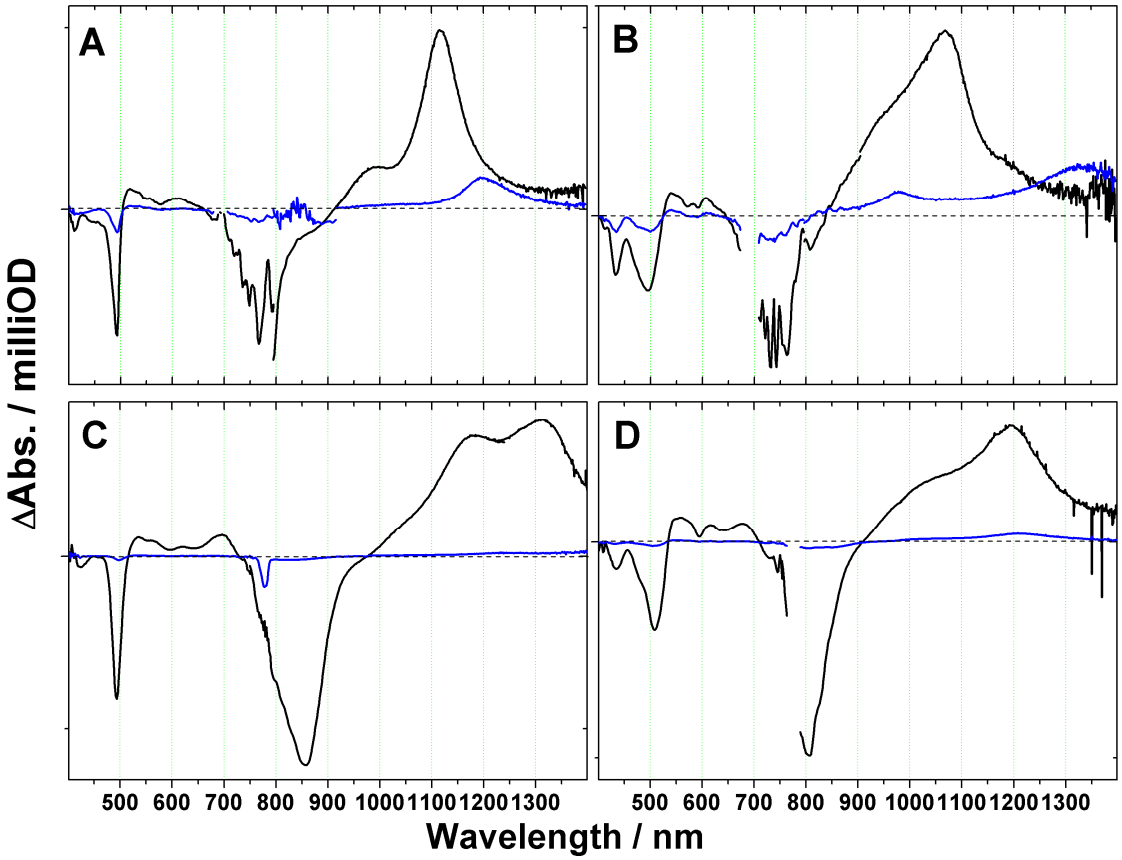
A
B
C
D
ΔAbs. / milliOD
500 600 700 800 900 1000 1100 1200 1300
500 600 700 800 900 1000 1100 1200 1300
Wavelength / nm

Figure S4

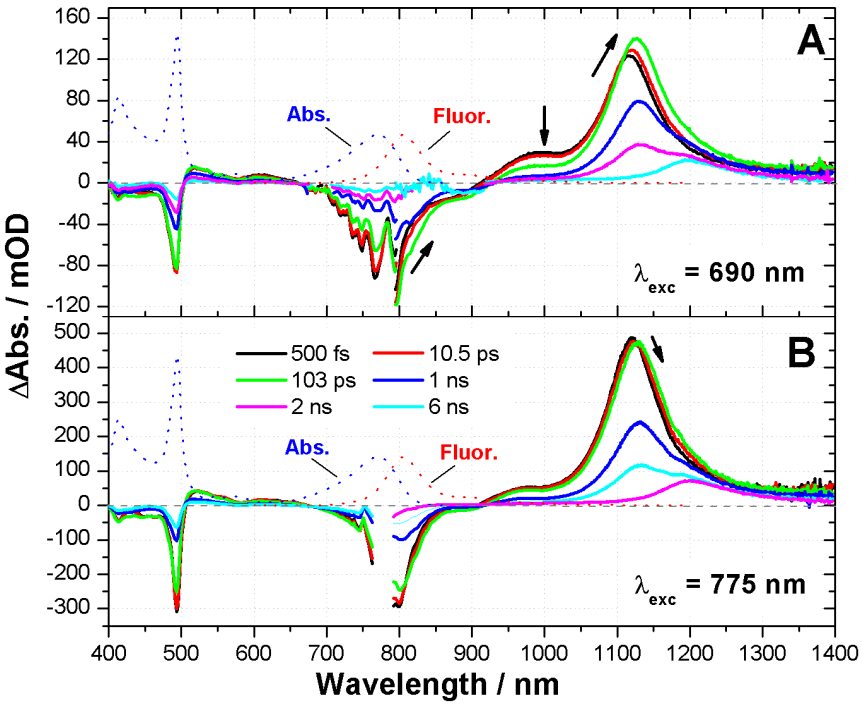
A
B
Abs.
Fluor.
Abs.
Fluor.
500 fs
10.5 ps
103 ps
1 ns
2 ns
6 ns
λexc = 690 nm
λexc = 775 nm
ΔAbs. / mOD
Wavelength / nm

Figure S5.

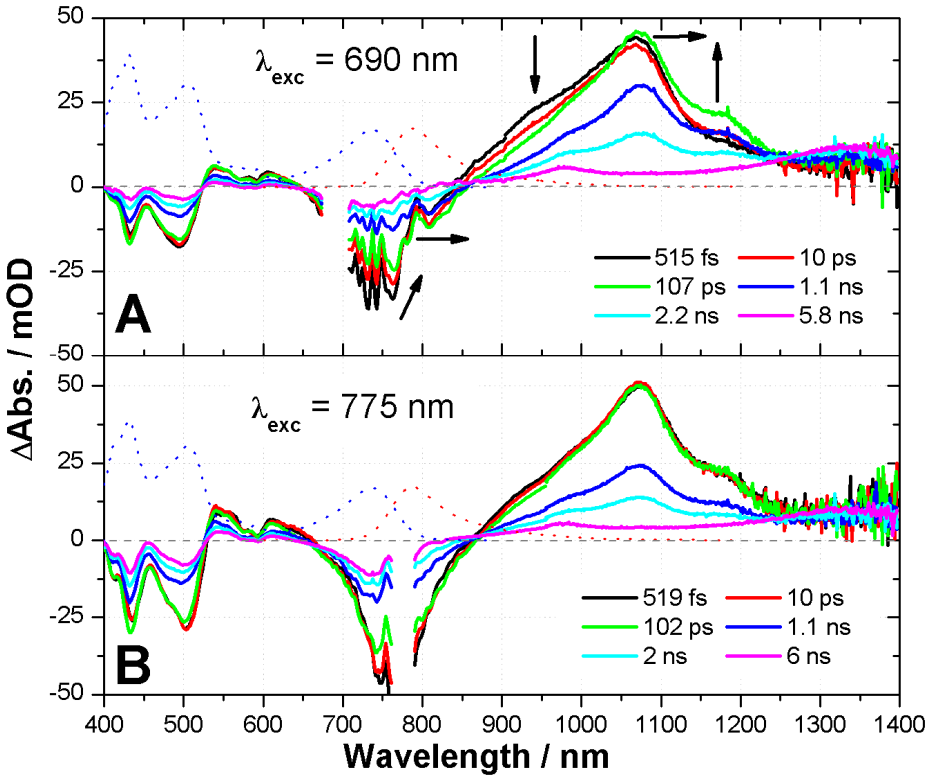
λexc = 690 nm
515 fs
10 ps
107 ps
1.1 ns
2.2 ns
5.8 ns
A
λexc = 775 nm
519 fs
10 ps
102 ps
1.1 ns
2 ns
6 ns
B
ΔAbs. / mOD
Wavelength / nm
50
25
0
-25
-50
400
500
600
700
800
900
1000
1100
1200
1300
1400

Figure S6

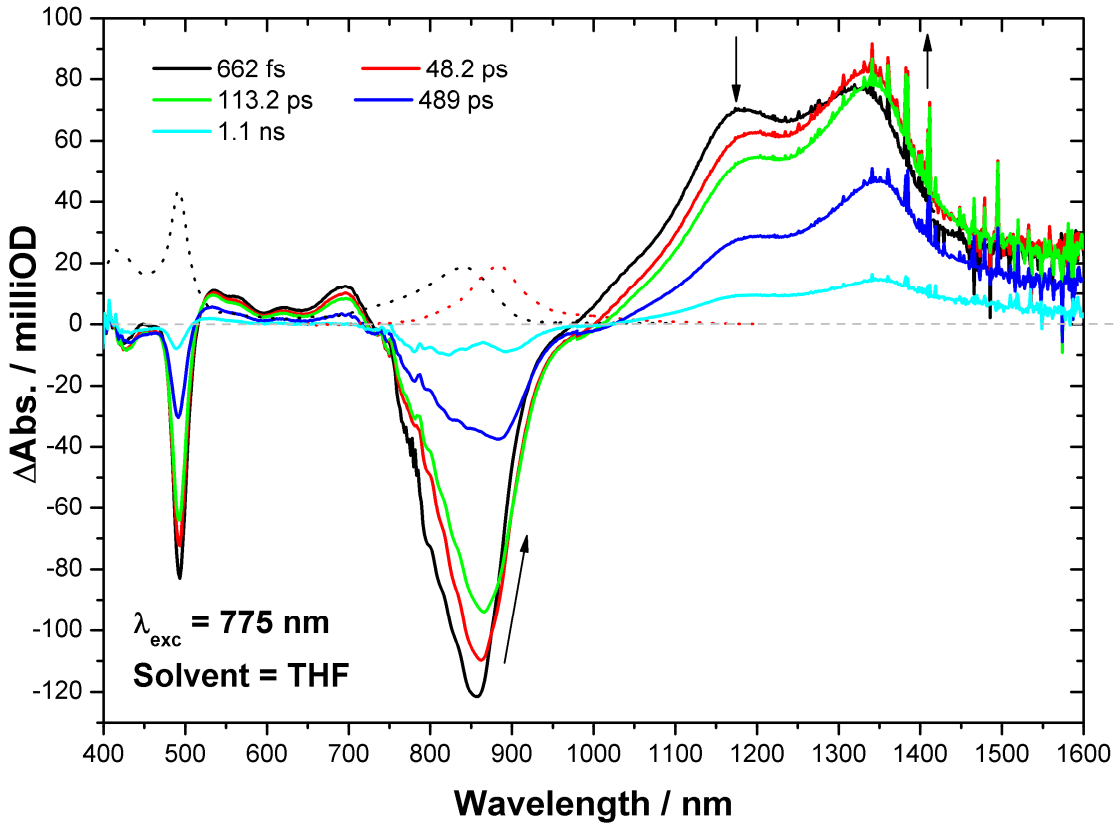
662 fs
48.2 ps
113.2 ps
489 ps
1.1 ns
λexc = 775 nm
Solvent = THF
ΔAbs. / milliOD
Wavelength / nm
100
80
60
40
20
0
-20
-40
-60
-80
-100
-120
400
500
600
700
800
900
1000
1100
1200
1300
1400
1500
1600

Figure S7

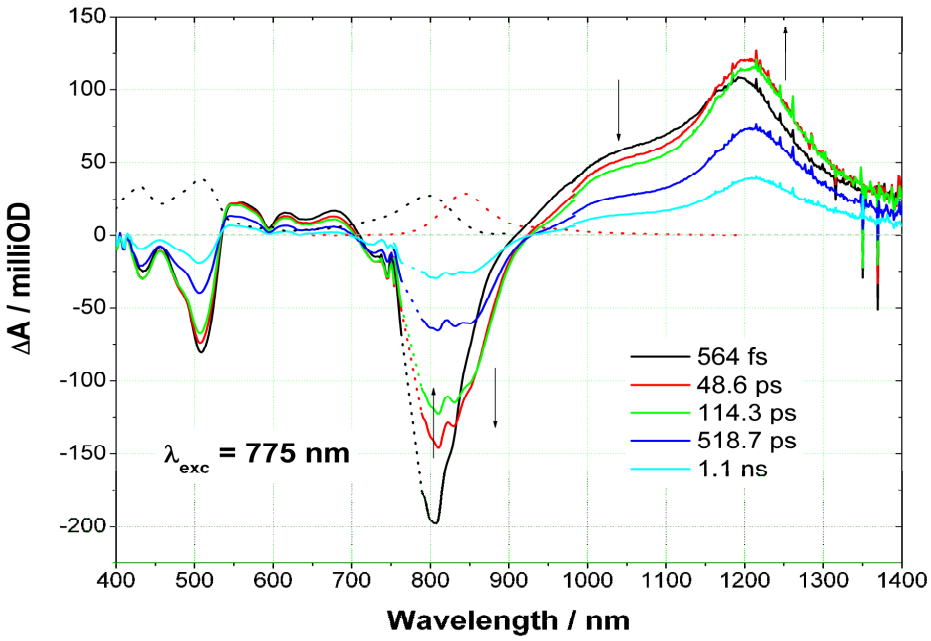
150
100
50
0
-50
-100
-150
-200
400
500
600
700
800
900
1000
1100
1200
1300
1400
ΔA / milliOD
Wavelength / nm
λexc = 775 nm
564 fs
48.6 ps
114.3 ps
518.7 ps
1.1 ns

Figure S8